ACS Energy LETTERS

Cite This: ACS Energy Lett. 2018, 3, 1165−1171

LETTER

Two-Dimensional Flexible Bilayer Janus Membrane for Advanced Photothermal Water Desalination

Yanbing Yang,[†,∥,#] Xiangdong Yang,[†,#] Linna Fu,[†] Mingchu Zou,[⊥] Anyuan Cao,[⊥] Yaping Du,[‡] Quan Yuan,[*,†] and Chun-Hua Yan[‡,§]

[†]Molecular Science and Biomedicine Laboratory, State Key Laboratory of Chemo/Biosensing and Chemometrics, College of Chemistry and Chemical Engineering, Hunan University, Changsha 410082, China

[‡]College of Chemistry, School of Materials Science and Engineering, National Institute for Advanced Materials, Nankai University, Tianjin 300350, China

[§]Beijing National Laboratory for Molecular Sciences, State Key Laboratory of Rare Earth Materials Chemistry and Applications, PKU−HKU Joint Laboratory in Rare Earth Materials and Bioinorganic Chemistry, College of Chemistry and Molecular Engineering, Peking University, Beijing 100871, China

[∥]Key Laboratory for Micro-/Nano-Optoelectronic Devices of Ministry of Education, School of Physics and Electronics, Hunan University, Changsha 410082, China

[⊥]Department of Materials Science and Engineering, College of Engineering, Peking University, Beijing 100871, China

Supporting Information

ABSTRACT: Solar water evaporation is thought to be a promising solution to address the issues of global water scarcity. However, it is particularly difficult to achieve an idealized photothermal conversion membrane with all of the required structure characteristics such as wide spectrum absorption, ultrathin and porous, low thermal conductivity, and ease to scale up, thus leading to reduced water evaporation efficiency. Here, we designed a large-area bilayer Janus film by assembling gold nanorod (AuNR) onto the interconnected single-walled carbon nanotube (SWNT) porous film. The combined characteristics of high solar spectrum absorption, enhanced photothermal performance, thermal insulating feature, interconnected porous structure, and excellent mechanical performance enable the bilayer Janus film with a nearly 94% water evaporation efficiency under 5 kW m^{-2} solar irradiation and stable water generation capability during long-term illumination cycles as a water desalination membrane. Construction of the bilayer Janus film represents an effective strategy for developing multifunctional membranes for advanced desalination applications.

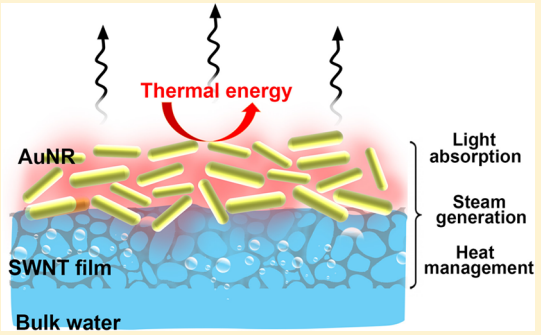

The shortage of available drinking water resources is known to be a serious global problem, especially in urban and rural areas.[1−3] Harvesting of abundant solar energy and then converting it to heat for steam generation is one of the most economical sustainable technologies for efficient seawater desalination and purification.[4−9] Recently, research on solar-enabled desalination has focused on localized heating of interfacial water for solar vapor generation based on nanomaterials with light absorption capabilities such as noble metallic nanoparticles,[10,11] polypyrrole organic polymers,[12] and carbon-based nanomaterials.[13−22] The concept of localized heating can localize the high temperature at the water−air interface and generate a sharp temperature gradient to decrease the heat loss caused by energy transfer to the nonevaporative portion of bulk water, eventually resulting in improved evaporation efficiency. Typically, an ideal photothermal conversion material for localized heating should possess several distinct characteristics, including: (1) broad-band absorption capability and low reflection in the full solar spectrum range;[21,23] (2) an ultrathin and interconnected porous structure for fluid and steam pass through;[24] (3) low thermal conductivity to suppress thermal transport to the non-evaporation part;[25] and (4) ease to scale up.[26] Thus far, photothermal membranes based on various designs such as carbon foam supported graphite,[14] graphene oxide,[15] TiO_x,[27,28]

Received: March 18, 2018
Accepted: April 20, 2018
Published: April 20, 2018

DOI: 10.1021/acsenergylett.8b00433
ACS Energy Lett. 2018, 3, 1165−1171

self-assembled metal nanostructure,[29−31] and polypyrrole-coated stainless steel mesh[12] have been developed, and their applications in solar steam generation have been exploited. Despite tremendous advancements of localized heating materials for steam generation, in practical applications, the overall vapor generation capability and water production capacity require further improvement. The fundamental reason lies in the fact that it is difficult to obtain a localized photothermal membrane that can meet all of the demands of the required structural properties, consequently resulting in decreased steam generation efficiency and limiting the utilization of these materials in point-of-use solar thermal evaporation systems. We have previously reported an ultrathin SWNT-MoS_2 film with an interconnected porous network and wide spectrum absorption capability for high-efficiency solar steam generation,[32] while the limitation in synthesis conditions inhibits its large-area fabrication. To date, it is desirable but remains a great challenge to develop an efficient photothermal membrane with multifunctional characteristics in one component for high-efficiency water desalination.

Herein, we report the first example of constructing of bilayer two-dimensional (2D) Janus membrane based on a single-walled carbon nanotube (SWNT) film assembled with plasmonic Au nanorod (AuNR) as an efficient light absorber for solar-enabled evaporation (Scheme 1). In this system, the

Scheme 1. Schematic Diagram of the Water Evaporation Measurement with the Bilayer SWNT/AuNR Janus Film Floating on the Water Surface

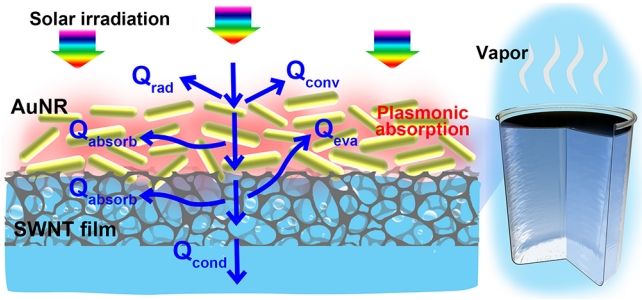

upper AuNR film serves as the plasmonic absorption layer and converts the absorbed solar light into thermal energy. The enormous pores present between the individual AuNR allow the fast transport of vapor. The underlying SWNT film with broad-band spectrum absorption not only enhances the solar spectrum absorption capability and improves the photothermal conversion efficiency but also acts as a mechanical supporting layer to maintain the structural integrity of the upper AuNR layer. At the same time, the SWNT film with an ultrathin and porous network structure (Figure S1) provides a pathway for continuous transport of water and vapor. This interconnected porous structure also serves as a thermal barrier layer to alleviate heat loss to the bulk water and confines heat at the evaporative surface. Consequently, the optimized SWNT/AuNR bilayer structure can significantly increase the evaporation efficiency (Q_{eva}) by minizing the conduction heat loss (Q_{cond}) to the underlying water as well as the convection (Q_{conv}) and radiation losses (Q_{rad}) toward the ambient environment[5] (Supporting Information, SI-1). As a localized solar steam generation membrane, the bilayer SWNT/AuNR film achieves a nearly 94% evaporation efficiency under 5 kW m^{-2} solar irradiation. In addition, benefiting from the excellent mechanical strength of the SWNT film, the bilayer membrane maintains a stable structure and excellent evaporation efficiency for at least 24 illumination cycles. It is worth mentioning that this is the first demonstration of a large-area and ultrathin bilayer Janus membrane with an interconnected porous structure and all-in-one properties for high efficiency and portable water desalination. This bilayer structure provides a concept of constructing a new-type multifunctional membrane to harvest renewable solar energy for a broad range of applications associated with energy resource.

The bilayer SWNT/AuNR Janus film, which is composed of an assembled AuNR top layer sitting on the surface of a SWNT supporting network, is fabricated by depositing an AuNR solution directly onto the SWNT film (Figures 1a and S2). The bilayer SWNT/AuNR Janus film with a diameter of 2.2 cm is ultrathin and appears black in color, as indicated in the cross-sectional photograph of the bilayer SWNT/AuNR film (Figure 1b). The assembled AuNR layer sitting on the SWNT film as well as the interface can be evidenced by the magnified scanning electron microscopy (SEM) image in Figure 1c. The seamless interface between the two layers indicates that the AuNR layer has a strong adhesion and interfacial interaction with the SWNT networks. Also, the protruded SWNTs in the SWNT layer suggest that the SWNT film exhibits excellent flexibility and mechanical stability, which is responsible for the mechanical integrity of the entire film. The SEM image of the top surface of the bilayer SWNT/AuNR film shown in Figure 1d indicates that the assembled AuNR layer is continuous in a large area. The connections between the AuNR domains are similar to the mountain ridges and valleys (Figure S3), demonstrating that the SWNT/AuNR film exhibits high surface roughness. The magnified SEM image of the select white area in Figure 1d shows that the AuNR layer is composed of randomly distributed AuNR with a length of 30 nm and width of 10 nm (inset of Figure 1d and Figure S4). This microscale surface structure of the SWNT/AuNR bilayer film can ensure intimate and maximized contact between the film and water, thus significantly promoting heat transfer from the bilayer film to water. From Figure 1e, it can be seen that the bottom layer of the SWNT/AuNR bilayer film is composed of fishing net-like interconnected SWNT networks with submicrometer scale pores. The pores that exist in the SWNT film as well as in the AuNR layer ensure that the bilayer film has sufficient pathways for efficient water and vapor transportation.

To evaluate the surface characteristic of the SWNT/AuNR film, the contact angle measurement was performed. As shown in Figure 2a, the contact angle of the uppper AuNR layer is measured to be 110°, and this surface hydrophobicity ensures the ultralight SWNT/AuNR film to have self-floating capability at the air−water interface as well as to benefit the self-sustained interfacial heating.[12] The bottom surface of the bilayer SWNT/AuNR film exhibits slightly hydrophilic behavior with a contact angle of 76°, which is attributed to the surface oxygen plasma treatment of SWNTs. This hydrophilic characteristic facilitates efficient fluid flow through the film toward the hot region as well as unimpeded vapor escaping. More importantly, the bilayer SWNT/AuNR Janus film is freestanding and can be easily handled by a tweezer (Figure 2b). Furthermore, Figure 2b shows that the bilayer SWNT/AuNR film can be freely bent to a large angle and even folded to a specific shape and maintains mechanical intactness. It is worth mentioning that the SWNT/AuNR film can be easily scaled up regarding the large-area fabrication of SWNT films (Figure 2c). The bilayer

DOI: 10.1021/acsenergylett.8b00433
ACS Energy Lett. 2018, 3, 1165−1171

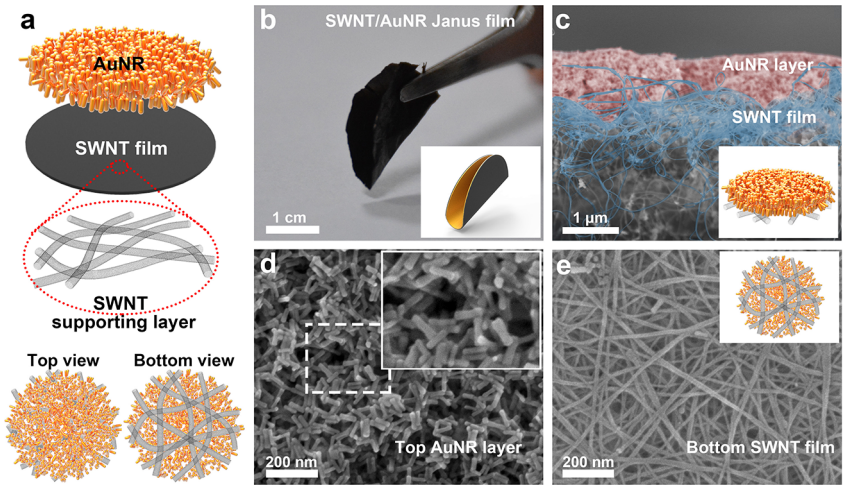

Figure 1. Structure of the bilayer SWNT/AuNR film. (a) Schematic structure of the bilayer SWNT/AuNR Janus film viewd from different angles. (b) Photograph of the bilayer SWNT/AuNR Janus film in the cross section direction. The inset of (b) is the structural model of the bilayer SWNT/AuNR film under bending conditions. (c) SEM image of the cross section of the bilayer SWNT/AuNR Janus film. The inset of (c) is the structural model of the bilayer SWNT/AuNR Janus film. (d) SEM image of the top surface of the bilayer SWNT/AuNR film. The inset of (d) is the magnified SEM image of the AuNR layer. (e) SEM image of the bottom surface of the bilayer SWNT/AuNR film. The inset of (e) is the structural model of the bottom surface of the SWNT/AuNR film.

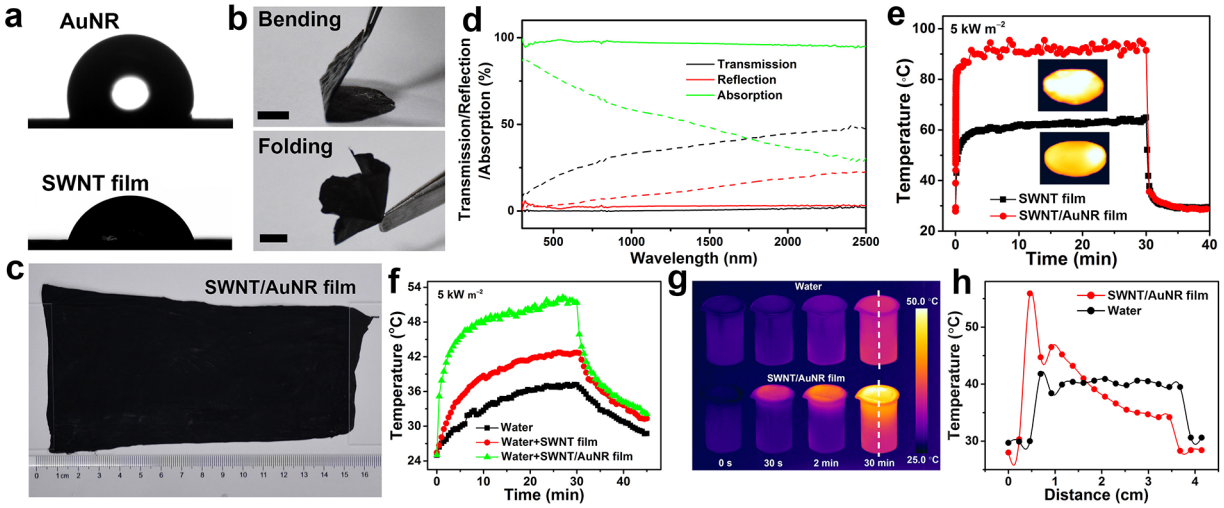

Figure 2. Surface properties and photothermal performance of the bilayer Janus film. (a) Contact angle of the bilayer Janus film. (b) Photograph of the SWNT/AuNR film handled by a tweezer and optical images of the SWNT/AuNR film under different deformations. Scale bars are 5 mm. (c) Photograph of the large-area SWNT/AuNR bilayer Janus film. (d) Optical properties of SWNT and SWNT/AuNR films in the wavelength range of 300−2500 nm. Dashed and solid lines represent SWNT and SWNT/AuNR films, respectively. (e) Time course of the surface temperature of the SWNT film and bilayer SWNT/AuNR film in air under solar power density of 5 kW m^{-2}. The insets of (e) are the IR thermal images of the SWNT and SWNT/AuNR films under solar irradiation for 10 min. (f) Time course of the surface temperature of pure water, the SWNT film, and the SWNT/AuNR film floating on the water surface under solar power density of 5 kW m^{-2}. (g) IR thermal images of water before light irradiation (0 s) and after light irradiation for 30 s and 2 and 30 min, respectively. Top beaker: pure water. Bottom beaker: water with the bilayer SWNT/AuNR film floating on the water surface. The solar irradiation power density is 5 kW m^{-2}. (h) Temperature profiles of the marked lines in (g).

SWNT/AuNR film can be stretched to large strains of 19% and is mechanically strong enough to sustain a stress of 28 MPa (Figure S5). The excellent mechanical flexibility is derived from the interconnected networks of the SWNT film as well as the high Young's modulus of the SWNT.[33] The excellent mechanical flexibility combined with the self-floating capability enables movement of the freestanding SWNT/AuNR Janus film along the water surface and facilitates automated interfacial water evaporation persistently and efficiently. The spectrum measurements were performed to evaluate the light absorption capability of our fabricated bilayer SWNT/AuNR film. As shown in Figure 2d, the bilayer SWNT/AuNR Janus film with a thickness of ∼1 μm exhibits a surprisingly negligible optical transmission (0.2%) and low reflection (1.8%) over the whole spectrum range of 300−2500 nm, corresponding to strong absorption of 98.0%. The high optical absorption of the bilayer film is due to the combined characteristic broad-band absorption of the AuNR film and SWNT layer as well as the large light scattering of nanoscale AuNR domains, which increases the optical path length in the bilayer film.[24] Meanwhile, the improved surface roughness (Figure S3), which enhances the multiscattering of incident light, is also a

DOI: 10.1021/acsenergylett.8b00433
ACS Energy Lett. 2018, 3, 1165−1171

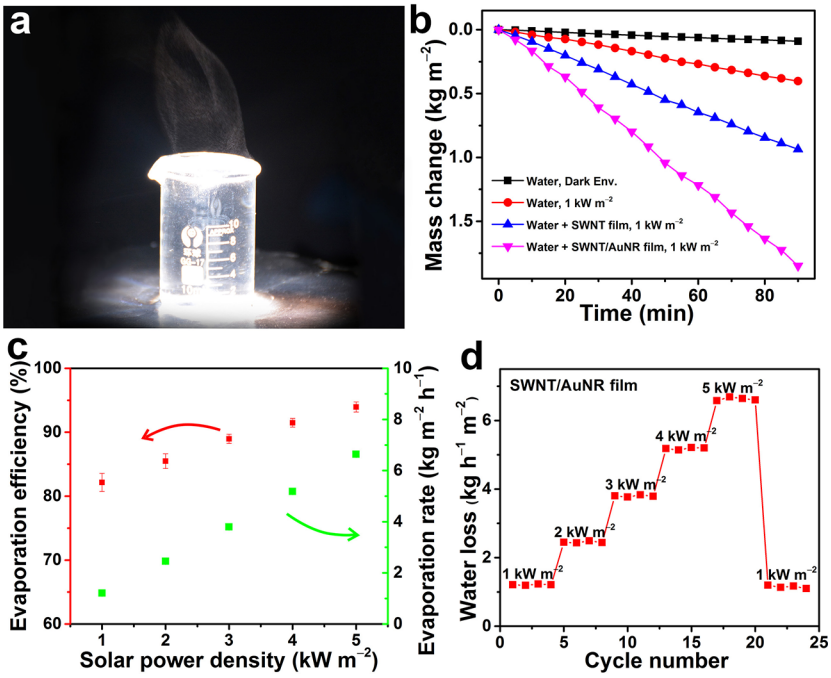

Figure 3. Solar steam generation performance of the bilayer SWNT/AuNR film. (a) Photograph of the water steam generated with the bilayer SWNT/AuNR Janus film floating on the water surface in a beaker. The solar power density was set at 5 kW m^{-2}. (b) Mass loss as a function of time under various conditions. Black: pure water under dark conditions. Red: pure water under 1 kW m^{-2}. Blue: water with the SWNT film under 1 kW m^{-2}. Pink: water with the bilayer SWNT/AuNR film under light irradiation of 1 kW m^{-2}. (c) Solar thermal conversion efficiency and evaporation rate of water with the bilayer SWNT/AuNR film under different solar power densities. (d) Evaporation rate versus cycle number under a series of solar power densities.

benefit for the effective absorption.[31] The high spectrum absorption capability of the SWNT/AuNR film is responsible for the high photothermal conversion efficiency.[31]

The photothermal performance of the SWNT/AuNR Janus membranes was investigated. As shown in Figure 2e, upon 5 kW m^{-2} light irradiation, the surface temperature of the bilayer SWNT/AuNR film quickly rises to 85 °C and then gradually increases to a steady-state temperature of 95 °C, while the pure SWNT film shows a relatively low temperature of 60 °C. This result demonstrates that the plasmonic heating was induced by the AuNR layer and resulted in improved photothermal conversion performance of the SWNT/AuNR film. Additionally, it also can be seen that the temperature distribution of the SWNT/AuNR film along the plane after 10 min of irradiation is homogeneous, illustrating that the AuNR are uniformly distributed on the SWNT film. The temperature distribution and thermal profiles of the bilayer SWNT/AuNR film floated on the water surface were also tested to evaluate the photothermal conversion performance under practical water evaporation conditions. As shown in Figure 2f, after 5 kW m^{-2} of light illumination for 30 min, the temperature of pure water slowly rises from room temperature to 37 °C. After incorporation of the SWNT film, the surface temperature increases to about 42.5 °C. In comparison, the temperature of the bilayer SWNT/AuNR film quickly elevates to 45 °C and eventually reaches to a steady-state temperature of 52 °C, which represents a 15 °C increment compared to that of pure water. More importantly, the SWNT/AuNR film exhibits excellent photothermal performance after several light irradiation cycles, as indicated in Figure S9, demonstrating that the bilayer film shows high stability due to the presence of a mechanically robust SWNT film. The IR images at different time periods were captured simultaneously to monitor the temperature distribution of water (Figure 2g). From the images, it can be seen that after light illumination for 30 min, an obvious hot planar image forms in the SWNT/AuNR film and the interfacial water temperature is immediately increased to as high as 52 °C. More importantly, in contrast with the uniform temperature distribution of pure water, a sharp temperature gradient is observed for water with a SWNT/AuNR film, demonstrating the heat localization effect of the bilayer SWNT/AuNR film (Figure 2h). In addition to the interfacial heating effect, the low thermal transport along the cross-plane of the film inhibits thermal diffusion from the film surface to bulk water, which is also responsible for the temperature gradient difference. The thermal conductivity of the SWNT/AuNR film saturated with water was measured to be 0.2 W m^{-1} K^{-1} (see the Experimental Details), which is lower than that of pure water (0.6 W m^{-1} K^{-1}).[34] This thermal conductivity is also comparable to the recently developed photothermal conversion materials that were employed in solar steam generation systems such as carbon foam supported graphite (0.959 W m^{-1} K^{-1}),[14] polystyrene foam (0.04 W m^{-1} K^{-1}),[15] airlaid paper (0.03−0.05 W m^{-1} K^{-1}),[31] and a cellulose supported GO membrane (0.816 W m^{-1} K^{-1})[25] with thicknesses in the range of 1−16 mm, which is much thicker than our fabricated bilayer SWNT/AuNR film (∼1 μm). Because the high porosity is responsible for the improved thermal conduction resistance,[20,35] the low thermal conductivity of the bilayer SWNT/AuNR film originates from the porous network structure of the SWNT film and AuNR layer. The heat loss including conduction, radiation, and convection loss of the system with the SWNT/AuNR film was calculated to be only 11.3% under 1 kW m^{-2} solar irradiation (Supporting Information, SI-1). The advantages of broad-band spectrum absorption, excellent photothermal conversion capability, thermal insulating features, as

DOI: 10.1021/acsenergylett.8b00433
ACS Energy Lett. 2018, 3, 1165−1171

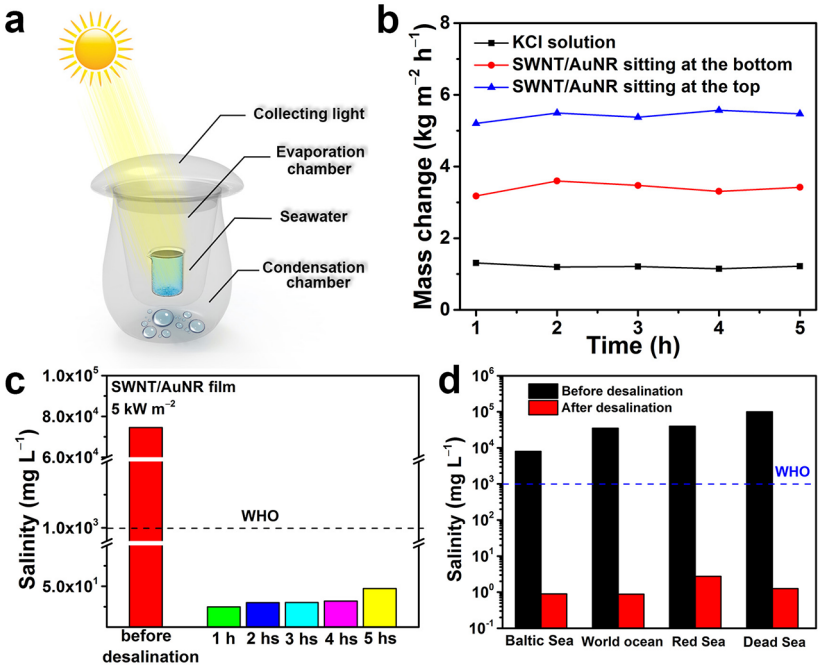

Figure 4. Point-of-use water desalination setup. (a) Schematic drawing of the point-of-use water desalination device for freshwater production. (b) Comparison of the water loss of the pure saline solution as well as the water loss of saline solution with a SWNT/AuNR film floating at the surface and sitting at the bottom of the beaker. The solar power density was set at 5 kW m^{-2}. (c) Measured salinity of the saline solution before and after different time periods of desalination. (d) Salinities of four simulated seawater samples before and after desalination. The dashed lines in (c) and (d) indicate the WHO standard for available water.

well as a porous network structure make such a bilayer SWNT/AuNR Janus film particularly suitable for solar-enabled evaporation and desalination processes.

The solar steam generation capability of our designed SWNT/AuNR bilayer film floating on the water surface was investigated under a series of simulated solar illumination power densities. From the photograph in Figure 3a, it can be seen that the steam can be clearly observed for water with a SWNT/AuNR film under a solar illumination power density of 5 kW m^{-2}, demonstrating the fast evaporation of water. The steam generation capability was quantified by measuring the mass change of water after a specific period of irradiation time. As shown in Figure 3b, the mass change of water increases linearly with irradiation time at different solar illumination densities. The mass change of water after solar irradiation (1 kW m^{-2}) for 90 min is 0.40 kg m^{-2}. The presence of a SWNT film increases the mass change of water to 0.94 kg m^{-2}, which is more than 1 time higher than that of pure water. Replacing the SWNT film with a bilayer SWNT/AuNR film leads to a significantly enhanced mass change of 1.85 kg m^{-2}, which represents 197% that of the SWNT film, demonstrating that the AuNR layer exhibits enhanced solar steam generation efficiency. It is worth mentioning that the mass change of water with the SWNT/AuNR film shows a consistent increase as the solar illumination power density increases from 1 to 5 kW m^{-2}, as shown in Figure 3c. The maximum evaporation rate of the SWNT/AuNR film is up to 6.7 kg m^{-2} h^{-1}. This evaporation rate is higher than that of the reported localized photothermal conversion material such as a flexible black Au film (3.0 kg m^{-2} h^{-1}),[24] carbon foam supported graphite (5.8 kg m^{-2} h^{-1}),[14] Ti_2O_3 nanoparticles (5.0 kg m^{-2} h^{-1}),[27] etc. The water evaporation efficiency (η) was calculated according to the following formula[24] to differentiate the photothermal performance of the film

$$\eta = \frac{\dot{m} \times h_{LV}}{I} \quad (1)$$

where $\dot{m}$ is the evaporation rate of the system, h_{LV} represents the total enthalpy of sensible heat (315 kJ kg^{-1}, from 25 to 100 °C with specific heat of 4.2 kJ kg^{-1}) and liquid−vapor phase change (~2260 kJ kg^{-1}), and I corresponds to the power density of solar irradiation. To precisely evaluate the evaporation efficiency, the evaporation rate in the dark environment is subtracted from all measured evaporation rates under solar irradiation. The evaporation efficiency as a function of solar irradiation power density is plotted in Figure 3c. From the curve, it is obvious that the evaporation efficiency of the bilayer SWNT/AuNR film (82%) under 1 kW m^{-2} solar irradiation is significantly higher than that of the SWNT film (46%) and pure water (19%). Additionally, the evaporation efficiency of the bilayer SWNT/AuNR film increases with the solar irradiation density in which the maximum evaporation efficiency reaches 94% under a solar irradiation power density of 5 kW m^{-2}. To our best knowledge, this evaporation efficiency ranks extremely high even compared with that reported under a solar irradiation power density higher than 5 kW m^{-2} (Tables S1 and S2). The durability of the SWNT/AuNR film was evaluated by exposing the film to cycling light irradiation conditions and recording the mass changes (Figure 3d). As evidenced in Figures 3d and S10, the bilayer SWNT/AuNR film shows a stable evaporation rate during the 24 irradiation cycles and maintains the structural integrity without performance degradation. In addition, the AuNR are firmly attached on the surface of the SWNT film before and after water evaporation cycles, as observed from the SEM images (Figure S10), suggesting excellent structure durability. The high evaporation efficiency as well as the reusability of the SWNT/AuNR film can be attributed to the following characteristics:

DOI: 10.1021/acsenergylett.8b00433
ACS Energy Lett. 2018, 3, 1165−1171

(1) the broad spectrum absorption and excellent photothermal conversion efficiency of the SWNT/AuNR film enables efficient heat generation; (2) the low thermal transport through the cross-plane suppresses thermal dissipation from the film surface to bulk water; (3) the SWNT network and AuNR layer both possess porous structures, which can provide a pathway for efficient water supply and vapor flow; (4) the outstanding mechanical flexibility of the SWNT/AuNR film enables intimate contact between the film with a fluctuating water surface, benefiting efficient water diffusion. Apart from the above-mentioned factors, it is anticipated that the evaporation efficiency of the bilayer SWNT/AuNR Janus film can be further improved through the design of an effective evaporation setup and engineering of an optimized microstructure.[36]

The designed freestanding and large-area SWNT/AuNR film shows great potential to be used for portable water desalination. In this regard, a portable solar desalination setup was designed to evaluate the water evaporation and desalination performance of the SWNT/AuNR film (Figure 4a, Figure S11). The device consists of an evaporation chamber located within the large condensation chamber. The bilayer SWNT/AuNR film floated on the surface of the saline water (KCl solution) is sitting at the evaporation chamber. Upon solar irradiation, the steam generated from the air−water interface escapes from the film and then condenses in the bottom condensation chamber. Figure 4b shows that the mass change of the KCl solution for the SWNT/AuNR film floated on the solution surface is measured to be 5.5 kg m^{-2}, significantly higher than that of a pure KCl solution (1.2 kg m^{-2}) and SWNT/AuNR film sitting at the bottom of the solution (3.5 kg m^{-2}). The conductivity of the collected water in the condensation chamber after different periods of desalination was measured, and it is observed that all of the salinities of the collected water have a remarkable reduction (10^3 orders) compared with the original KCl (Figure 4c). This salinity is also far below the salinity level defined by the World Health Organization (WHO), illustrating that the SWNT/AuNR film can serve as a highly efficient desalination membrane. The stable desalination performance of the film demonstrates that the salt residues on the film surface have a negligible influence on the long-term reusability of the film. Salt solutions with different salinities were employed as the representative seawater models (the Baltic Sea (0.8 wt %), the world ocean (3.5 wt %), the Red Sea (4 wt %), and the Dead Sea (10 wt %)) to explore the practical desalination applications of the SWNT/AuNR film (Figure 4d). It can be observed that all of the desalinated water shows extremely low salinity, suggesting that the SWNT/AuNR film exhibits excellent desalination performance irrespective of the salinity of seawater. The above results demonstrate that the designed bilayer SWNT/AuNR Janus film can effectively function as a photothermal membrane for practical point-of-use water desalination.

In summary, we have demonstrated a bilayer SWNT/AuNR Janus film for highly efficient solar water desalination. The bilayer SWNT/AuNR film exhibits high spectrum absorption ability and excellent photothermal conversion efficiency. The incorporation of the SWNT film enables the bilayer film with excellent mechanical flexibility, ensuring intimate contact between the film and the water surface and a benefit for efficient water diffusion. The SWNT/AuNR film localizes the heat on the evaporative surface and limits heat loss to the underlying bulk water. Meanwhile, the interconnected porous structure facilitates fast vapor transport. When employed as a localized heating membrane, the bilayer SWNT/AuNR film floated on the water surface reaches a high surface temperature of 52 °C and shows a surprisingly high water evaporation rate of 6.7 kg m^{-2} h^{-1}. Notably, the bilayer SWNT/AuNR film shows a stable water evaporation rate and high water evaporation efficiency (94%) even after recycling light irradiation. The concept of rational integration of a plasmonic photothermal membrane with an ultrathin and porous SWNT network to form the bilayer Janus film was embodied for the first time. We believe that this demonstration of a bilayer SWNT/AuNR film represents a promising strategy to construct advanced functional nanomaterials for portable water production technologies.

■ ASSOCIATED CONTENT

Supporting Information

The Supporting Information is available free of charge on the ACS Publications website at DOI: 10.1021/acsenergylett.8b00433.

Experimental details; SEM and TEM images of the SWNT film; 3D AFM image of the bilayer SWNT/AuNR Janus film; TEM image and UV−vis absorption spectrum of the AuNR; EDX spectra of the bilayer SWNT/AuNR Janus film; tensile stress−strain curve of the SWNT/AuNR film; time course of the surface temperatures of the SWNT/AuNR film at different solar irradiation power densities; IR thermal images of SWNT and SWNT/AuNR films; time course of the surface temperature of pure water, the SWNT film, and the SWNT/AuNR film floating on the water surface; photograph and SEM images of the SWNT/AuNR films before and after water evaporation; and photograph of the point-of-use solar water evaporation system (PDF)

■ AUTHOR INFORMATION

Corresponding Author

*E-mail: yuanquan@whu.edu.cn.

ORCID

Anyuan Cao: 0000-0002-2282-716X
Quan Yuan: 0000-0002-3085-431X
Chun-Hua Yan: 0000-0002-0581-2951

Author Contributions

#Y.Y. and X.Y. contributed equally to this work.

Notes

The authors declare no competing financial interest.

■ ACKNOWLEDGMENTS

This work was supported by the National Key Research and Development Program of China (2017YFA0208000), National Natural Science Foundation of China (21675120), Ten Thousand Talents Program for Young Talents, Start-up Research Fund for Prof. Q. Yuan (531107050973, 531109010053), and State Key Laboratory of Chemo/Biosensing and Chemometrics at Hunan University (732106172).

■ REFERENCES

(1) Elimelech, M.; Phillip, W. A. The future of seawater desalination: Energy, technology, and the environment. *Science* **2011**, 333, 712−717.

DOI: 10.1021/acsenergylett.8b00433
ACS Energy Lett. 2018, 3, 1165−1171

(2) Shannon, M. A.; Bohn, P. W.; Elimelech, M.; Georgiadis, J. G.; Mariñas, B. J.; Mayes, A. M. Science and technology for water purification in the coming decades. *Nature* **2008**, *452*, 301−310.
(3) Sun, P. Z.; Wang, K. L.; Zhu, H. W. Recent developments in graphene-based membranes: Structure, mass-transport mechanism and potential applications. *Adv. Mater.* **2016**, *28*, 2287−2310.
(4) Cartlidge, E. Saving for a rainy day. *Science* **2011**, *334*, 922−924.
(5) Deng, Z. Y.; Zhou, J. H.; Miao, L.; Liu, C. Y.; Peng, Y.; Sun, L. X.; Tanemura, S. The emergence of solar thermal utilization: Solar-driven steam generation. *J. Mater. Chem. A* **2017**, *5*, 7691−7709.
(6) Chen, C. J.; Li, Y. J.; Song, J. W.; Yang, Z.; Kuang, Y. D.; Hitz, E.; Jia, C.; Gong, A.; Jiang, F.; Zhu, J. Y.; et al. Highly flexible and efficient solar steam generation device. *Adv. Mater.* **2017**, *29*, 1701756.
(7) Xu, N.; Hu, X. Z.; Xu, W. C.; Li, X. Q.; Zhou, L.; Zhu, S. N.; Zhu, J. Mushrooms as efficient solar steam-generation devices. *Adv. Mater.* **2017**, *29*, 1606762.
(8) Li, R. Y.; Zhang, L. B.; Shi, L.; Wang, P. MXene Ti_3C_2: An effective 2D light-to-heat conversion material. *ACS Nano* **2017**, *11*, 3752−3759.
(9) Ni, G.; Li, G.; Boriskina, S. V.; Li, H. X.; Yang, W. L.; Zhang, T. J.; Chen, G. Steam generation under one sun enabled by a floating structure with thermal concentration. *Nat. Energy* **2016**, *1*, 16126.
(10) Fang, Z. Y.; Zhen, Y.-R.; Neumann, O.; Polman, A.; García de Abajo, F. J.; Nordlander, P.; Halas, N. J. Evolution of light-induced vapor generation at a liquid-immersed metallic nanoparticle. *Nano Lett.* **2013**, *13*, 1736−1742.
(11) Zhou, L.; Zhuang, S. D.; He, C. Y.; Tan, Y. L.; Wang, Z. L.; Zhu, J. Self-assembled spectrum selective plasmonic absorbers with tunable bandwidth for solar energy conversion. *Nano Energy* **2017**, *32*, 195−200.
(12) Zhang, L. B.; Tang, B.; Wu, J. B.; Li, R. Y.; Wang, P. Hydrophobic light-to-heat conversion membranes with self-healing ability for interfacial solar heating. *Adv. Mater.* **2015**, *27*, 4889−4894.
(13) Gao, X.; Ren, H. Y.; Zhou, J. Y.; Du, R.; Yin, C.; Liu, R.; Peng, H. L.; Tong, L. M.; Liu, Z. F.; Zhang, J. Synthesis of hierarchical graphdiyne-based architecture for efficient solar steam generation. *Chem. Mater.* **2017**, *29*, 5777−5781.
(14) Ghasemi, H.; Ni, G.; Marconnet, A. M.; Loomis, J.; Yerci, S.; Miljkovic, N.; Chen, G. Solar steam generation by heat localization. *Nat. Commun.* **2014**, *5*, 4449.
(15) Li, X. Q.; Xu, W. C.; Tang, M. Y.; Zhou, L.; Zhu, B.; Zhu, S. N.; Zhu, J. Graphene oxide-based efficient and scalable solar desalination under one sun with a confined 2D water path. *Proc. Natl. Acad. Sci. U. S. A.* **2016**, *113*, 13953−13958.
(16) Ito, Y.; Tanabe, Y.; Han, J. H.; Fujita, T.; Tanigaki, K.; Chen, M. W. Multifunctional porous graphene for high-efficiency steam generation by heat localization. *Adv. Mater.* **2015**, *27*, 4302−4307.
(17) Zeng, Y.; Yao, J. F.; Horri, B. A.; Wang, K.; Wu, Y. Z.; Li, D.; Wang, H. T. Solar evaporation enhancement using floating light-absorbing magnetic particles. *Energy Environ. Sci.* **2011**, *4*, 4074−4078.
(18) Peng, L.; Xu, Z.; Liu, Z.; Guo, Y.; Li, P.; Gao, C. Ultrahigh thermal conductive yet super flexible graphene films. *Adv. Mater.* **2017**, *29*, 1700589.
(19) Zhang, H. Ultrathin two-dimensional nanomaterials. *ACS Nano* **2015**, *9*, 9451−9469.
(20) Li, Y. J.; Gao, T. T.; Yang, Z.; Chen, C. J.; Luo, W.; Song, J. W.; Hitz, E.; Jia, C.; Zhou, Y. B.; Liu, B. Y.; et al. 3D-printed, all-in-one evaporator for high-efficiency solar steam generation under 1 sun illumination. *Adv. Mater.* **2017**, *29*, 1700981.
(21) Zhang, P. P.; Li, J.; Lv, L. X.; Zhao, Y.; Qu, L. T. Vertically aligned graphene sheets membrane for highly efficient solar thermal generation of clean water. *ACS Nano* **2017**, *11*, 5087−5093.
(22) Li, X. Q.; Lin, R. X.; Ni, G.; Xu, N.; Hu, X. Z.; Zhu, B.; Lv, G. X.; Li, J. L.; Zhu, S. N.; Zhu, J. Three-dimensional artificial transpiration for efficient solar waste-water treatment. *Natl. Sci. Rev.* **2018**, *5*, 70−77.
(23) Zhou, L.; Tan, Y. L.; Wang, J. Y.; Xu, W. C.; Yuan, Y.; Cai, W. S.; Zhu, S. N.; Zhu, J. 3D self-assembly of aluminium nanoparticles for plasmon-enhanced solar desalination. *Nat. Photonics* **2016**, *10*, 393−398.
(24) Bae, K.; Kang, G. M.; Cho, S. K.; Park, W.; Kim, K.; Padilla, W. J. Flexible thin-film black gold membranes with ultrabroadband plasmonic nanofocusing for efficient solar vapour generation. *Nat. Commun.* **2015**, *6*, 10103.
(25) Jiang, Q. S.; Tian, L. M.; Liu, K. K.; Tadepalli, S.; Raliya, R.; Biswas, P.; Naik, R. R.; Singamaneni, S. Bilayered biofoam for highly efficient solar steam generation. *Adv. Mater.* **2016**, *28*, 9400−9407.
(26) Wang, Z. Z.; Ye, Q. X.; Liang, X. B.; Xu, J. L.; Chang, C.; Song, C. Y.; Shang, W.; Wu, J. B.; Tao, P.; Deng, T. Paper-based membranes on silicone floaters for efficient and fast solar-driven interfacial evaporation under one sun. *J. Mater. Chem. A* **2017**, *5*, 16359−16368.
(27) Wang, J.; Li, Y. Y.; Deng, L.; Wei, N. N.; Weng, Y. K.; Dong, S.; Qi, D. P.; Qiu, J.; Chen, X. D.; Wu, T. High-performance photothermal conversion of narrow-bandgap Ti_2O_3 nanoparticles. *Adv. Mater.* **2017**, *29*, 1603730.
(28) Ye, M. M.; Jia, J.; Wu, Z. J.; Qian, C. X.; Chen, R.; O'Brien, P. G.; Sun, W.; Dong, Y. C.; Ozin, G. A. Synthesis of black TiO_x nanoparticles by Mg reduction of TiO_2 nanocrystals and their application for solar water evaporation. *Adv. Energy Mater.* **2017**, *7*, 1601811.
(29) Zhou, L.; Tan, Y. L.; Ji, D. X.; Zhu, B.; Zhang, P.; Xu, J.; Gan, Q. Q.; Yu, Z. Y.; Zhu, J. Self-assembly of highly efficient, broadband plasmonic absorbers for solar steam generation. *Sci. Adv.* **2016**, *2*, e1501227.
(30) Zhou, L.; Tan, Y. L.; Wang, J. Y.; Xu, W. C.; Yuan, Y.; Cai, W. S.; Zhu, S. N.; Zhu, J. 3D self-assembly of aluminium nanoparticles for plasmon-enhanced solar desalination. *Nat. Photonics* **2016**, *10*, 393−398.
(31) Liu, Y. M.; Yu, S. T.; Feng, R.; Bernard, A.; Liu, Y.; Zhang, Y.; Duan, H. Z.; Shang, W.; Tao, P.; Song, C. Y.; et al. A bioinspired, reusable, paper-based system for high-performance large-scale evaporation. *Adv. Mater.* **2015**, *27*, 2768−2774.
(32) Yang, X. D.; Yang, Y. B.; Fu, L. N.; Zou, M. C.; Li, Z. H.; Cao, A. Y.; Yuan, Q. An ultrathin flexible 2D membrane based on single-walled nanotube-MoS_2 hybrid film for high-performance solar steam generation. *Adv. Funct. Mater.* **2018**, *28*, 1704505.
(33) Yu, M.-F.; Lourie, O.; Dyer, M. J.; Moloni, K.; Kelly, T. F.; Ruoff, R. S. Strength and breaking mechanism of multiwalled carbon nanotubes under tensile load. *Science* **2000**, *287*, 637−640.
(34) Ramires, M. L. V.; Nieto de Castro, C. A.; Nagasaka, Y.; Nagashima, A.; Assael, M. J.; Wakeham, W. A. Standard reference data for the thermal conductivity of water. *J. Phys. Chem. Ref. Data* **1995**, *24*, 1377−1381.
(35) Xu, W. C.; Hu, X. Z.; Zhuang, S. D.; Wang, Y. X.; Li, X. Q.; Zhou, L.; Zhu, S. N.; Zhu, J. Flexible and salt resistant Janus absorbers by electrospinning for stable and efficient solar desalination. *Adv. Energy Mater.* **2018**, *8*, 1702884.
(36) Ren, H. Y.; Tang, M.; Guan, B. L.; Wang, K. X.; Yang, J. W.; Wang, F. F.; Wang, M. Z.; Shan, J. Y.; Chen, Z. L.; Wei, D.; et al. Hierarchical graphene foam for efficient omnidirectional solar-thermal energy conversion. *Adv. Mater.* **2017**, *29*, 1702590.

DOI: 10.1021/acsenergylett.8b00433
ACS Energy Lett. 2018, 3, 1165−1171